

RESEARCH

Open Access



Implementation of direct battery driven discharge in triggerless operation of vacuum arc thrusters

James Saletes^{1*}, Kash Saddul¹, Alexander Wittig¹ and Minkwan Kim¹

*Correspondence:
J.Saletes@soton.ac.uk

¹ University of Southampton,
University Road,
Southampton SO17 1BJ, UK

Abstract

The increasing demand for CubeSat missions with limited budgets and constrained timelines necessitates the development of innovative propulsion systems. This paper focuses on vacuum arc thrusters (VATs) and investigates the implementation of battery-driven discharge for triggerless firing. VATs offer a promising alternative for CubeSat propulsion, generating thrust through the pulsed ejection of plasma in a cathode arc discharge. The study explores the feasibility of direct battery-driven discharge in VATs and demonstrates stable and variable-duration pulses. Experimental testing using high C-rating lithium-ion (Li-ion) batteries showcase the advantages and operational benefits of this approach. The results highlight the potential for variable energy pulses, precise control of thrust impulse bit, and improved performance compared to capacitor-driven systems. Future research directions include optimising pulse duration for enhanced lifetime, plume analysis, and erosion rate investigations. The implementation of VATs with battery-driven discharge presents a promising solution to enhance the performance and reliability of CubeSat propulsion systems while ensuring compliance with space sustainability guidelines.

Keywords: Vacuum arc thruster, Micro propulsion, Battery driven cathode arc, Triggerless

Introduction

Ever-increasing access to space is driving an upswing in CubeSat missions. CubeSats are subject strict volumetric (10 cm× 10 cm×10 cm per Unit), mass (1.33 kg per Unit), power (as low 2 W for a one Unit system) and regulatory constraints [1]. Adapting established spacecraft propulsion systems to meet these constraints presents significant challenges. For example, Hall effect thrusters, require increasingly stronger magnetic fields to confine the electrons within their annular channel, with a reduction in its diameter [2]. Hence it is difficult to scale down to the CubeSat level. Commonly used cold gas thrusters have a typically low specific impulse (ISP) of around 25–50 s [3], and chemical propulsion is constrained by the prohibition of pyrotechnic devices and the requirement to not exceed a pressure greater than 100 psi [1]. This has driven research into alternative means of propulsion tailored for implementation within the CubeSat ecosphere.

An appropriate choice for CubeSat propulsion would need to fit within these constraints, while being reliable and at a low cost. One such technology is the vacuum arc thruster (VAT). VATs generate thrust through the pulsed ejection of plasma produced through a cathode arc discharge under vacuum conditions [4]. The intense joule heating caused by high current densities at the cathode spot, the origin point of the arc, locally vaporises the cathode material at the cathode surface. Localised melting from the cathode spot forms cathode craters and surface droplets. This vaporised material is ionised within the arc by the stream of electrons, resulting in the formation of plasma. A combination of thermal expansion and electrostatic forcing from the potential slump at the positive sheath of the cathode spot expels arc plasma [5]. Figure 1 provides a schematic of this plasma formation and ejection from the cathode surface and a scanning electron microscope (SEM) image of a copper cathode after vacuum arc testing. Secondary acceleration mechanisms such as a magnetic field [6] or charged grid [7] can then be implemented to improve propellant and total efficiencies.

VATs offer extensive power scalability, from below the power generation capability of a 1U CubeSat through reducing the frequency or energy of the pulses, up to the power generation or thermal dissipation capacity a satellite. Theoretically, any conductive material can be used as the cathode (and thus the propellant). The VAT system is mechanically simple, requiring no moving parts and the propellant (cathode) is stored as a solid. These inherent advantages at the system level have led to the development of vacuum arc ignition methods compatible with CubeSat constraints. This was achieved through reduction of the breakdown voltage requirements through the concept of “triggerless” ignition, enabling the electronics to fit within the CubeSat form factor. This work was pioneered by André Anders et al., which utilises a thin conductive layer between the electrodes to allow for micro discharges to form across the insulator [8]. This concept was further developed by J. Schein et al., introducing inductive-driven storage to provide the desired pulse profile [9]. Figures 2 and 3 illustrate the principal schematic of this firing mechanism and the resultant pulse profile. Subsequent VAT systems incorporate

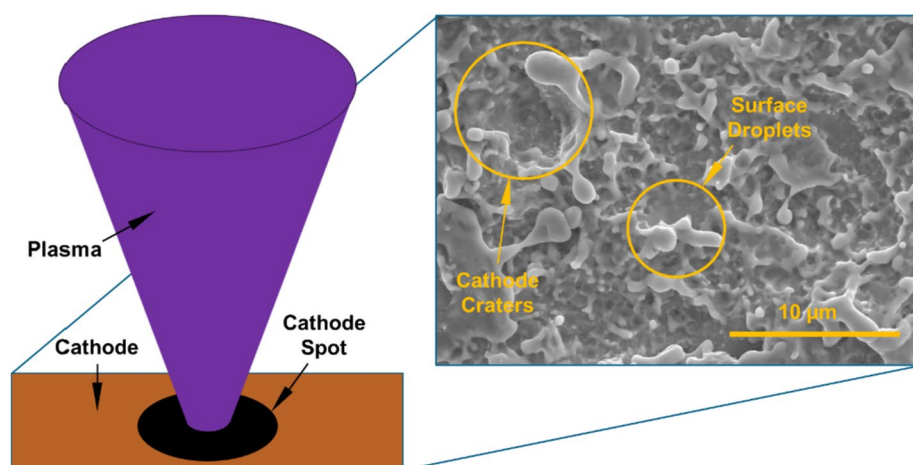


Fig. 1 Schematic of plasma formation and ejection within the cathode spot. SEM image of copper cathode after vacuum arc discharge showing cathode craters and surface droplets taken at the University of Southampton

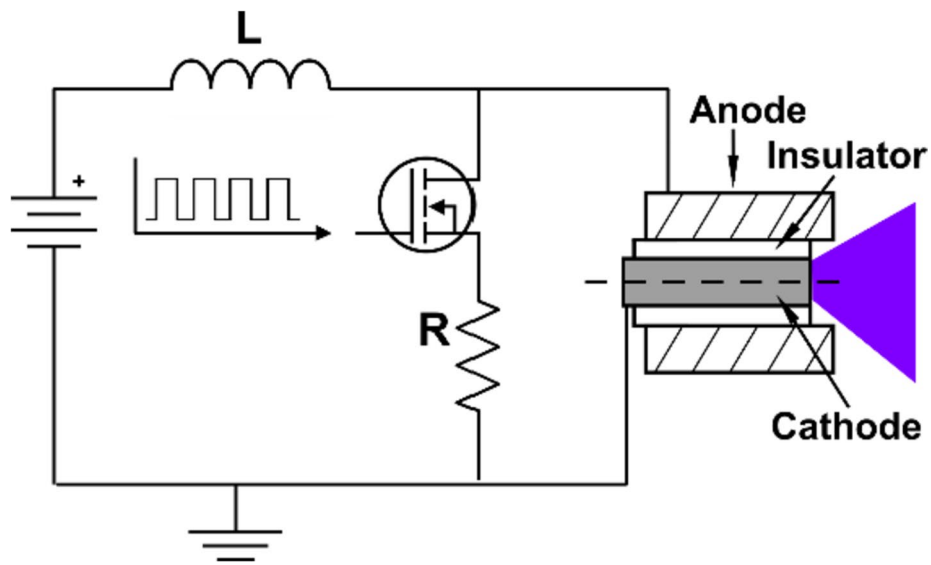


Fig. 2 Principle schematic of the coaxial vacuum arc assembly driven by inductive energy storage PPU

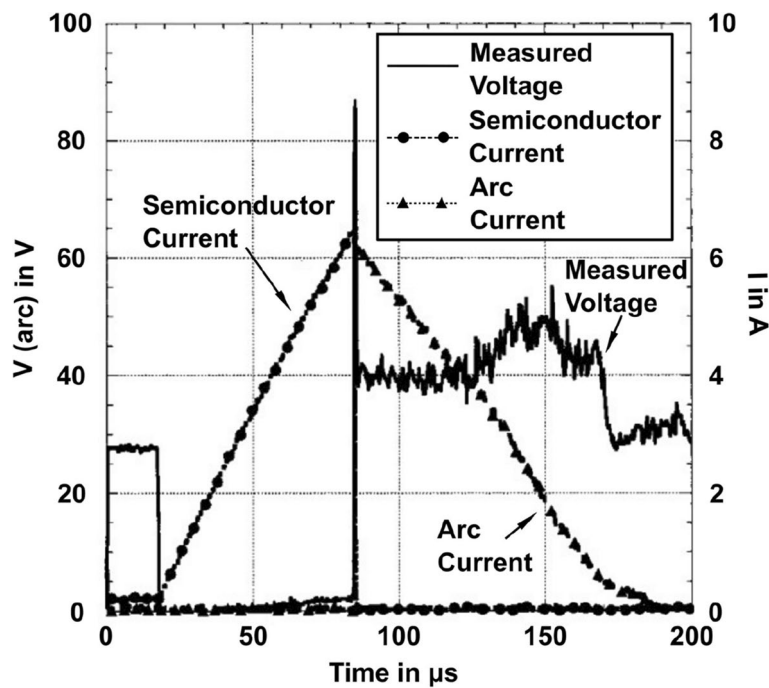


Fig. 3 Measured voltage (thick solid), current passing through the semiconductor switch (dashed with dots), and the arc current (dotted with triangles) of a tungsten arc [9]

capacitive storage into the power processing unit (PPU) to sustain the arc after plasma ignition [10, 11].

Optimal replenishment of the carbon layer is essential for triggerless operation of a VAT. During the cathode arc discharge, a proportion of the ions within the plasma return to the electrode surface and replenish the conductive layer [7]. Higher pulse powers (55–60 A for 510 μs) have been shown to lead to excessive replenishment, resulting

in a short circuit, while lower pulse powers (20–25 A for 1350 μ s) deplete the conductive layer faster than it is replenished [12]. The sustained operation of a VAT relying on a triggerless firing mechanism necessitates both reliable ignition and consistent pulse characteristics. The magnitude of the impulse bit, the measure of momentum change created by the VAT during one pulse, produced by a VAT is linearly driven by the total charge in the arc discharge, with higher charge levels yielding a greater impulse bit [7].

Implementing a low thrust VAT into a CubeSat would facilitate higher altitude missions while ensuring compliance with the IADC guidelines, de-orbiting within 25 years of end-of-life (EoL). Figure 4 presents simulation data from an orbital and attitude simulator developed by the University of Southampton [13] demonstrating the effect of increasing the longevity of a 10 μ N propulsion system on a 1U (10 \times 10 cm, 1.33 kg) on the time it takes for the spacecraft to de-orbit. For example, a 1 U CubeSat would become IADC in-compliant at around 665 km, but by thrusting for six months at 10 μ N, the time is decreased dramatically to 1.4 years. Hence, increasing the operational lifetime and reliability of the VAT technology is of crucial interest from the perspective of space sustainability [14].

One avenue of development to improve the operational lifetime of VAT systems is through the implementation of high C-rating Li-ion batteries capable of directly sustaining the vacuum arc, without reliance in internal energy storage of the PPU. Controlling

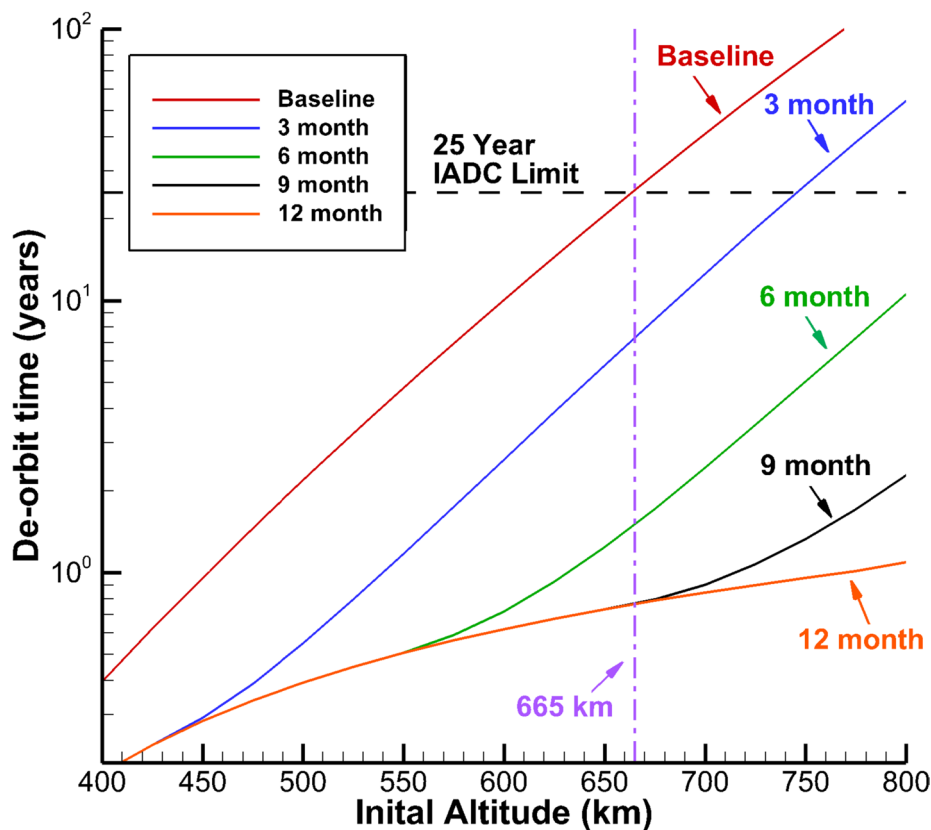


Fig. 4 De-orbiting time for a 1.33 kg initial mass 1U CubeSat from a given altitude with different continuous thrust times at 10 μ N

this discharge would enable modulation of the pulse energy and hence impulse bit without changing the hardware (typically the capacitor and inductor size). Pulse energies could hence be tailored to condition of the VAT to improve lifetime. Lithium-ion (Li-ion) batteries were first used in space as part of the 1994 Clementine mission to power its secondary payload, the Near-Infrared Mapping Spectrometer [15]. Subsequently, the space sector has been transitioning to adopt the technology over legacy nickel-hydrogen (Ni-H₂) batteries, taking advantage of their higher energy densities, typically 260–270 Wh/kg for Li-ion and approximately 140 Wh/kg for Ni-H₂ [16]. The ISS replaced its Ni-H₂ batteries in a series of spacewalks between 2017 and 2020 [17], and a wide selection of commercial off-the-shelf (COTS) Li-ion batteries are now available for CubeSat missions [18]. High C-rating and energy density Li-ion batteries have facilitated a rapid expansion in electric vehicle and unmanned aerial vehicle (UAV) markets over the past two decades [19, 20], with the Ingenuity UAV deploying across the surface of Mars in April 2021 using COTS Li-ion batteries [21].

This paper presents a novel implementation utilizing high C-rating Li-ion batteries to enable direct battery-driven discharge for triggerless firing VAT. The experimental setup is described in detail, and the results of both battery and capacitor-driven discharges, along with the end-of-life (EoL) mechanism experienced during battery-driven discharge, are discussed. This research offers new possibilities for VAT operation in space missions.

Experimental setup

The experiments were conducted on VATs under pressure less than 1×10^{-4} mbar using a PPU capable of delivering either capacitive or battery-driven discharge. Figure 4 illustrates the simplified schematic of the PPU and equipment setup. The PPU used is at the breadboard model phase of development and so does not comprise entirely of vacuum rated components. Hence, the electronics and diagnostic equipment were placed outside of the vacuum chamber. The VATs tested consisted of two planar polished copper electrodes measuring $2 \text{ mm} \times 10 \text{ mm} \times 5 \text{ mm}$, with 0.5 mm thick MACOR insulator separating them. Multiple NovaCentrix jr-700lv carbon ink [22] layers were applied onto the insulator until the resistance between the electrodes was $5 \text{ k}\Omega \pm 2 \text{ k}\Omega$. For capacitor-driven discharge, the power source was a 50 V power supply with an input resistance of $5 \text{ k}\Omega$. Energy was stored internally by a 470 μF capacitor to charge a 150 μH inductor and sustain the arc discharge. A 50 V lithium-ion battery pack capable of delivering a sustained current of 165 A was directly connected to the same PPU for battery-driven discharge.

The controller in Fig. 5 drives two insulated-gate bipolar transistors (IGBT), IGBT1 (IXYS corporation, IXYH10N170CV1) and IGBT2 (IXYS corporation, IXYH10N170CV1). IGBT1 enables the charging of the inductor by connecting it to ground when the controller sends a high “charging-signal”, and the IGBT2 connects the cathode to ground when the controller sends a high “out-signal”. At the initiation of the pulse ($t = 0$), both the charging and out-signals transition from low to high. Around 30 μs , the charging signal is brought low, while the out signal remains high. The rapid change in current caused by severing the inductor’s continuity to ground generates the necessary voltage spike for triggerless ignition. In the case of capacitor-driven

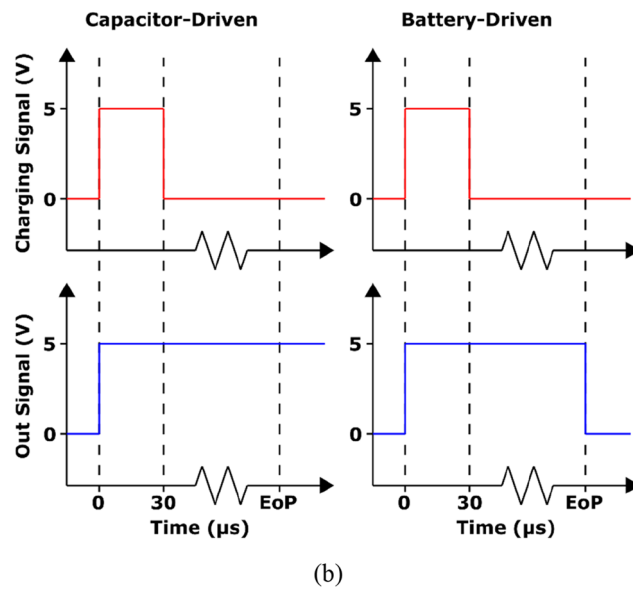
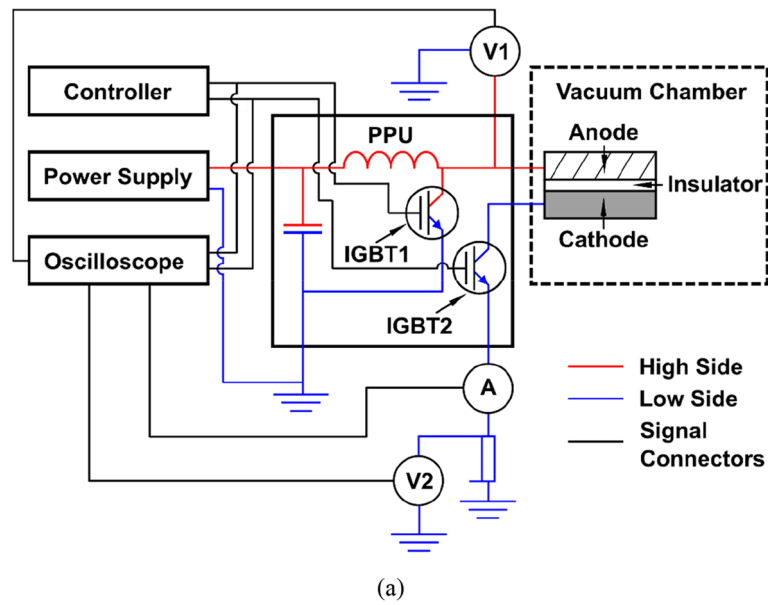


Fig. 5 **a** Simplified schematic of the PPU electronics and equipment configuration. **b** Signal protocol for the charging signal and out signal for capacitor-driven and battery-driven discharge up until end of pulse (EoP)

discharge, the out signal remains high throughout and beyond the full duration of the pulse. For battery-driven discharge, the out signal is brought low at the desired endpoint of the pulse, allowing for direct modulation of the pulse duration by varying the duty cycle of the out signal. A schematic of this signal protocol is shown in Fig. 5b.

Discharge current was measured directly through an inductive probe (A in Fig. 5) for the initial 15–20 μs of any given pulse. Beyond this timeframe, the probe readout dropped to zero as it reached the current-time limit. The direct current measurement data was utilised to calibrate the indirect current measurement obtained through the shunt resistor in Fig. 5. A dataset comprising more than 1100 pulses encompassing

battery and capacitor-driven discharge of four VATs was employed to derive a calibration constant of 20.4 mV/A with a standard deviation of 0.81 mV/A (3.89 %).

Four test VATs, namely VAT1, VAT2, VAT3 and VAT4, were subjected to different test protocols. VAT 1 testing predominantly focused on battery-driven discharge, and its results are discussed in Sect. 3. On the other hand, VAT2, VAT3 and VAT4 underwent capacitor-driven firing until they reached their defined capacitor end-of-life (EoL) condition. Subsequently, battery-driven discharge was employed on these VATs until it reached the battery EoL condition.

Capacitor-driven discharge

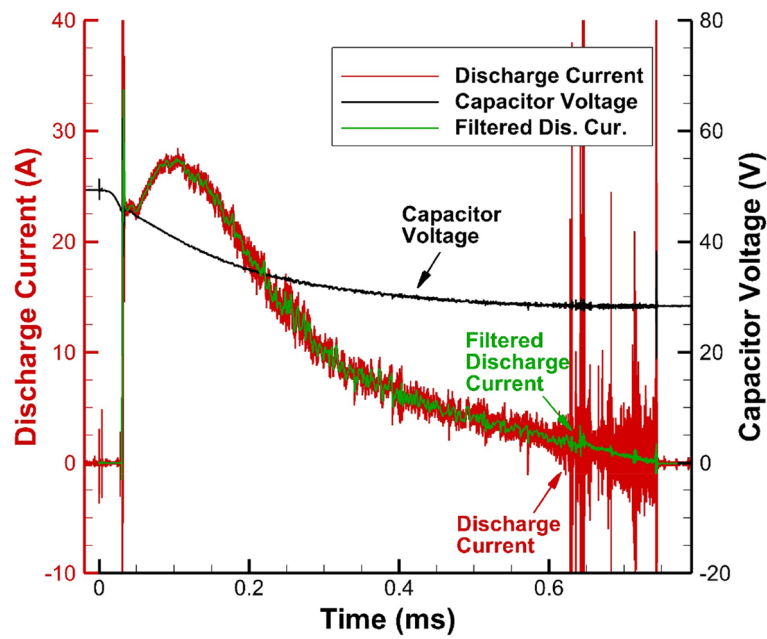
The capacitor-driven EoL condition was the occurrence of five consecutive pulse discharges that were not sustained by energy stored in the capacitor. Once breakdown occurs, the arc can be sustained either by the energy stored in the capacitor (as depicted in Fig. 6a) or solely by the remaining energy stored in the inductor (as shown in Fig. 6b). A moving average filter of window size 51 has been applied to the discharge current and plotted in Fig. 6. This condition is indicated when the voltage across the capacitor at the end of the pulse exceeds its initial value at the start of the arc discharge.

The number of pulses achieved before the EoL condition varied significantly among the tested VATs: 236 pulses for VAT2, 116 pulses for VAT3 and 304 pulses for VAT4. The discrepancy suggests variation in the distribution of the conductive layer among the VATs. Figure 7a and b illustrate the total charge distribution of the first and last 20 pulses, respectively, for VAT2 to VAT4. The error bars in the figures represent one standard deviation the uncertainty in the calibration of the discharge current. Comparing Fig. 7a and b, it is evident that the latter exhibits a greater charge distribution, with pulses of a lower total charge occurring. Pulses with a lower charge provide a lower impulse bit, indicating a reduction and variation in the performance of the VAT as it approaches its EoL.

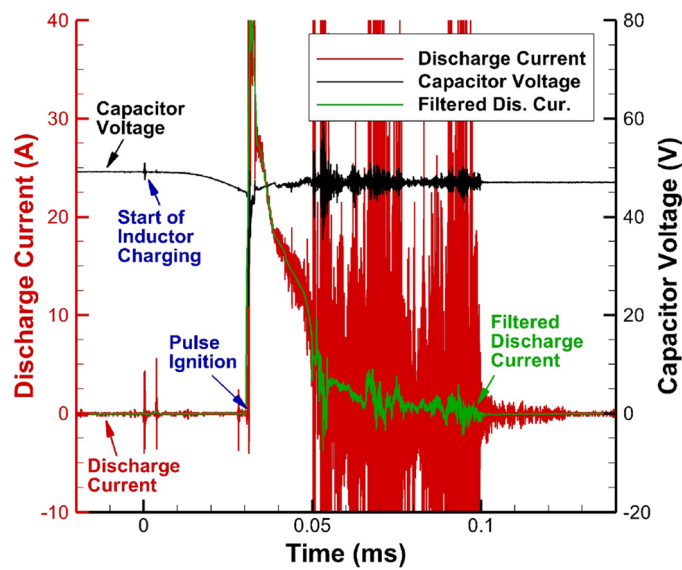
Battery-driven discharge

Battery-driven discharge testing of VAT1 varied the out-signal duration between 1 ms and 12 ms at 1 ms intervals. Figure 8a – d present the pulse profile of 3 ms, 6 ms, 9 ms and 12 ms respectively, with annotated high and low out-signal regions. Triggerless ignition occurs around $t = 30 \mu\text{s}$, where the discharge current rapidly increases to its maximum over the first 0.1 ms as plasma establishes across the VAT. By $t = 0.3$ ms, the discharge current stabilises at a reduced level of approximately 30 A. Resistance across circuit-protecting components (mechanical switch, fuse and Schottky diode), as well as in the wiring and connectors, creating a higher resistive path between the battery and VAT compared to the capacitor and the VAT. Hence, the initial current hump greater than 30 A is attributed to energy being supplied from the capacitor. After this point, the discharge current is solely driven by the battery. Once the out-signal is brought low, the IGBT gate voltage drops, causing the discharge current to decay to zero.

Figure 9 illustrates the total charge accumulated in each of the battery-driven discharges, with the error bars representing the uncertainty in the calibration of the shunt resistor. In Fig. 9a, the dashed line represents a linear relationship passing through (0,0) with a gradient of 30.05 C/s. The data points align closely with this



(a)



(b)

Fig. 6 Discharge current and capacitor voltage during capacitor-driven firing of VAT2. **a** First pulse. **b** Final capacitor-driven pulse

line resulting in a high coefficient of determination (R^2) of 0.996. This implies that extending the pulse duration exhibits a direct and linear correlation with the total charge delivered during the battery-driven pulse. The cathode mass eroded, and so the impulse bit, are directly proportional to the charge in the discharge current [7], allowing for precise control over thrust.

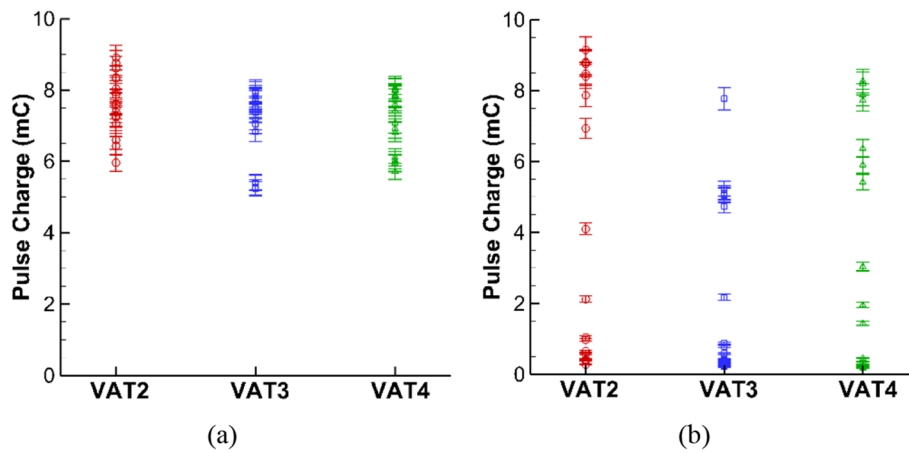


Fig. 7 Total charge per capacitor-driven pulse for VAT2, VAT3 and VAT4. **a** First 20 pulses for VAT2, VAT3 and VAT4. **b** Final 20 pulses for VAT2, VAT3 and VAT4

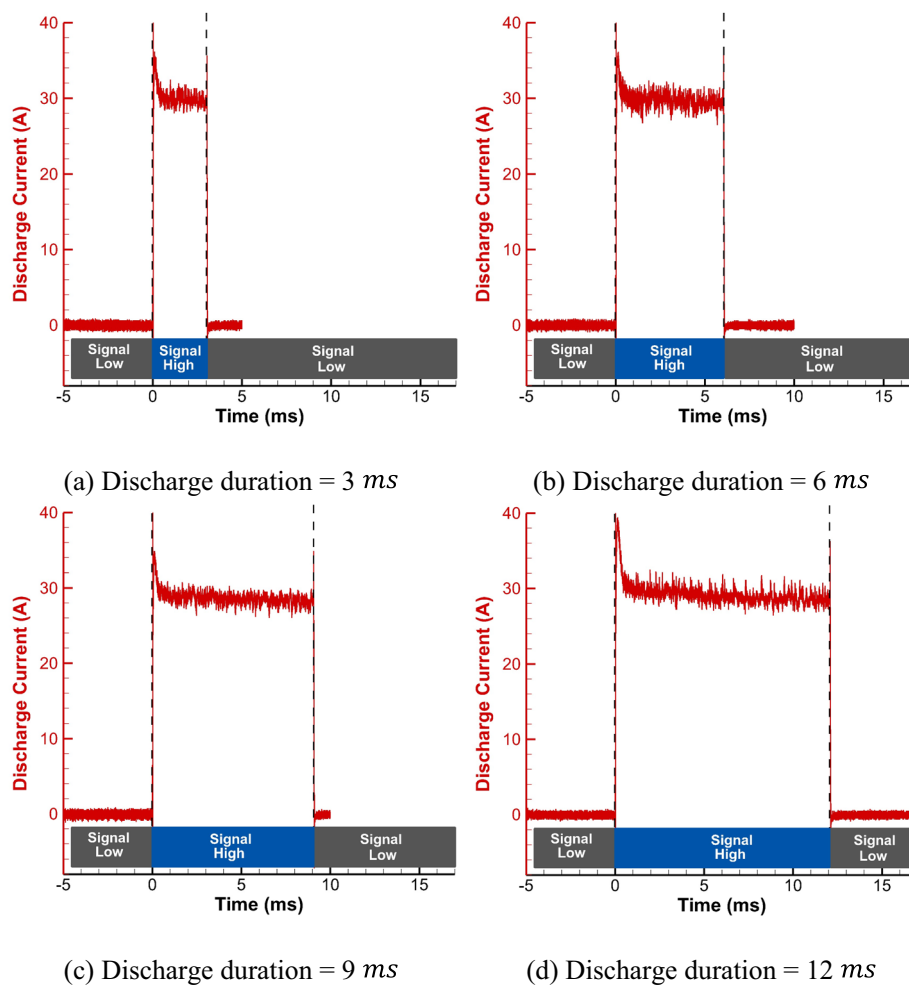


Fig. 8 Discharge current of battery-driven discharge with annotated high and low signal regions. **a** 3 ms pulse. **b** 6 ms pulse. **c** 9 ms pulse. **d** 12 ms pulse

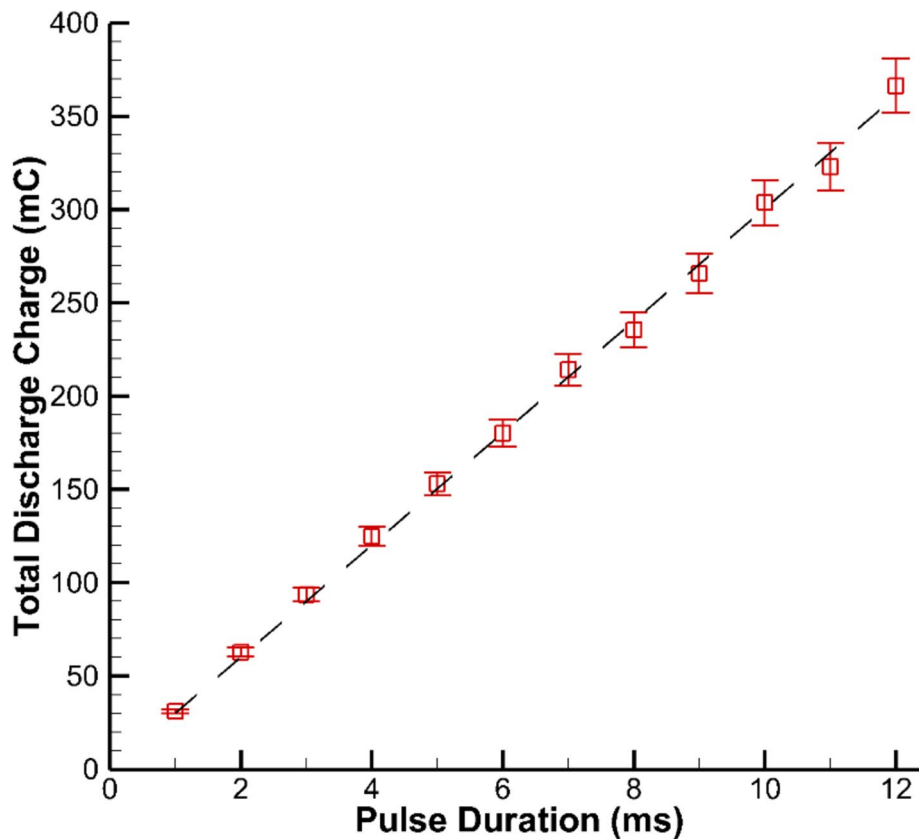


Fig. 9 Total charge in the battery-driven discharge for 1 ms to 12 ms

Figure 10 showcases a collage of Digital Single-Lens Reflex (DLSR) images captured during each of the 12 discharges. Images were taken using a D5600 camera, with a Tamron Sp 90 mm f/2.8 Di MACRO 1:1 lens, set to an ISO setting of 400, an aperture of F32, and an exposure of 3 s. Observing the images, it becomes apparent that as the duration of the discharge increases, the plasma appears brighter and occupies a larger volume within the frame. Additionally, starting from 4 ms pulse duration and onwards, an increasing rate of formation of macroparticles is observed. The macroparticles are molten droplets composed of un-ionised electrode or insulator material. Their presence signifies a degradation in the structure of the VAT and indicates a reduction of the efficiency of the propellant utilisation.

Battery-driven EoL

VAT2 to VAT4 were subjected to 3 ms battery-driven discharges after the capacitor-driven EoL condition until five consecutive pulses did not sustain a discharge current for the duration of the high out-signal. As with the number of pulses delivered before the capacitor EoL, the number of pulses delivered before the battery-driven EoL condition was met varied significantly. VAT2 achieved 141 battery-driven pulses, of which nine did not sustain current for 3 ms. VAT3 achieved 43 battery-driven pulses, of which 20 did not sustain current for 3 ms. VAT4 achieved 80 battery-driven pulses, of which 22 did not sustain current for 3 ms. Each case represented a significant extension of the life

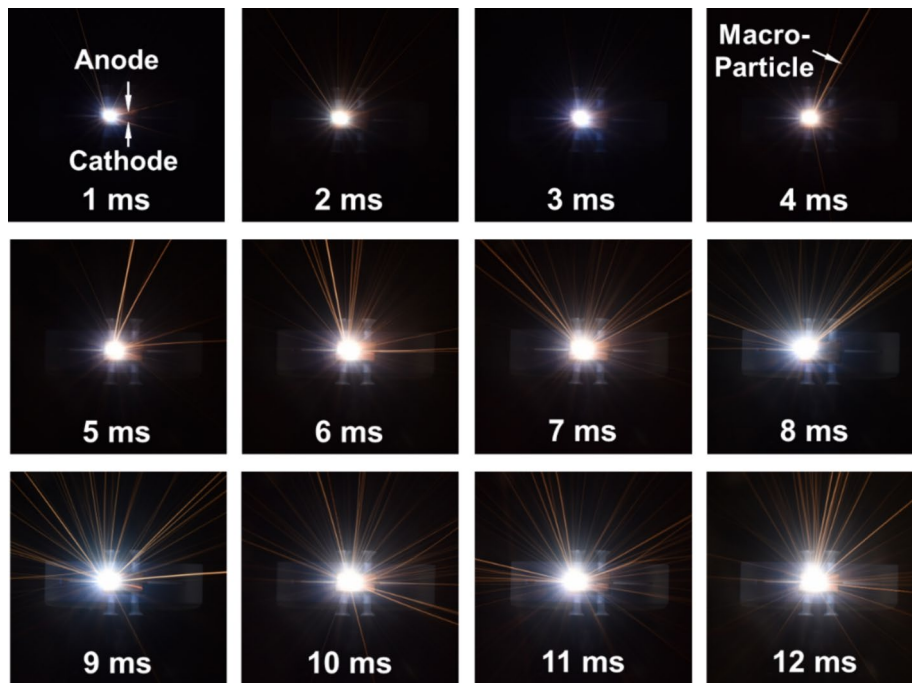
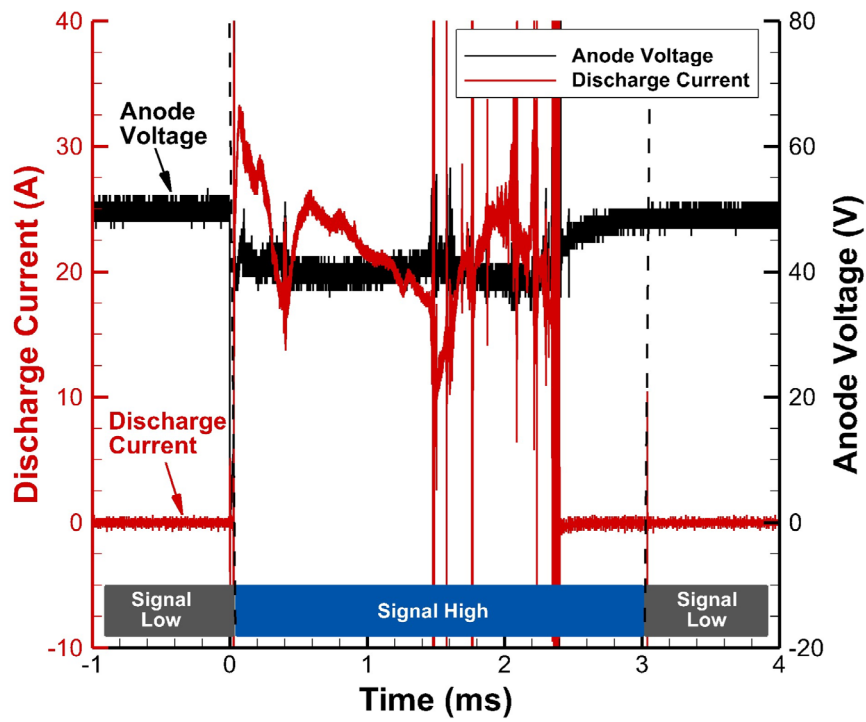


Fig. 10 DSLR images of battery-driven discharge of VAT1 with ascending pulse duration between 1 *ms* and 12 *ms*.

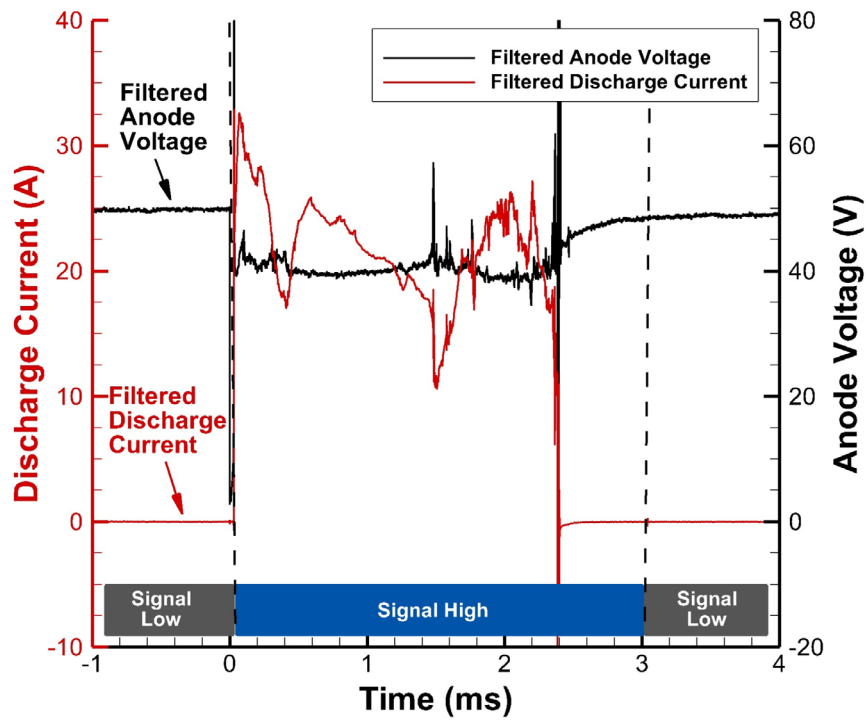
of the VAT, with each sustained 3 *ms* discharges delivering an order of magnitude more energy than the capacitor-driven discharges.

Discharge current was passed through the inductor in the PPU before reaching the VAT. This allows stabilisation of the arc as a reduction in discharge current translates to a change in current at the inductor, producing a voltage spike. This voltage spike allows for the potential reignition of the discharge during the pulse, with this effect becoming prevalent as the VAT approaches its end of life. Figure 11, the pulse profile of the 54th batter-driven discharge of VAT4, clearly demonstrated this effect with reductions in the discharge current at 0.4 *ms* and 1.5 *ms* resulting in voltage spikes at the anode that cause a resurgence in the discharge current. Increasing the size of the inductor would strengthen this stabilising effect but risks a sudden drop in the discharge current triggering a high voltage spike that could damage the electronics while adding mass and increasing electromagnetic noise within the confined CubeSat budgets.

Figure 12 highlights the physical degradation of VAT2 from battery-driven discharge. Figure 12a provides an image schematic of VAT2 before testing, and Fig. 12b provides an exploded image of the same VAT in atmosphere after its battery EoL condition. The image shows an extensive reduction in the carbon layer and the exposure of the MACOR insulator between the electrodes. This reduction was caused by the melting and macro-particle ejection of the surface of the MACOR insulator (which remains structurally stable up to 1000 °C under zero load [23]), taking the carbon layer with it. This suggests that the lifetime of the VAT could be enhanced through a reduction in the pulse duration, reducing the of joule heating. Moreover, incorporating an insulator with a higher melting point, such as alumina (melting point: 2072 °C [24]) as compared to copper



(a)



(b)

Fig. 11 Pulse profile of the 54th battery driven discharge of VAT4 with annotated high and low signal regions. **a** Unfiltered anode voltage (red) and discharge current (black) data. **b** Unfiltered anode voltage (red) and discharge current (black) data

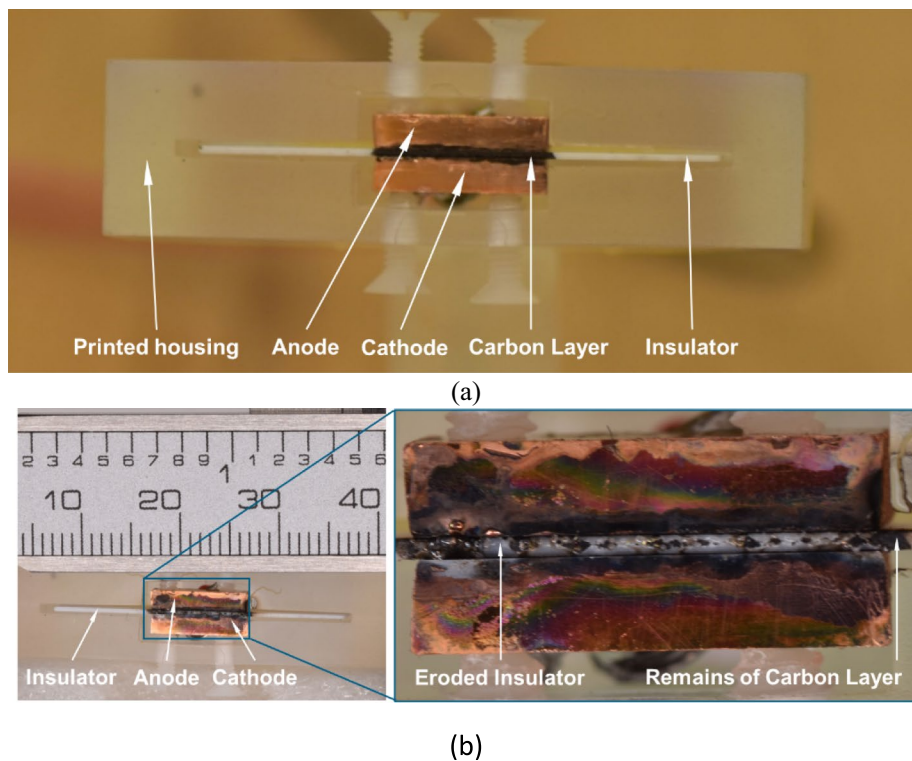


Fig. 12 DSLR images of VAT2. **a** Image taken before vacuum firing. **b** Image taken after battery driven EoL. LHS, electrode schematic with ruler mm/ inch ruler for scale. RHS, exploded image of the electrodes

electrodes (melting point: 1085 °C) could ensure that cathode erosion, rather than insulator erosion, occurs.

Conclusion

Implementing battery-driven discharge for triggerless VATs has been demonstrated as a viable approach to achieve stable and variable-duration pulses. This study presented data for pulse durations up to 12 ms. However, the potential for even higher durations was observed, with the limiting factor in the current design being the fuse into the PPU. Battery-driven discharges also exhibited greater discharge stability, maintaining a discharge current at 30 A and dropping to zero once the out signal is dropped low. This is in contrast to the noisy decay to zero over the pulse duration, seen by the capacitor-driven discharge.

This research's findings open avenues for future investigations in the field of VATs. Firstly, it would be valuable to determine the optimum pulse duration for a given electrode and insulator material to maximise the system's lifetime. Higher energy discharges could facilitate plume analysis or direct measurement of the impulse bit. Furthermore, investigating the effect of pulse energy on erosion rates would provide insights into the erosion mechanisms and contribute to optimising the thruster's propellant efficiency.

From an operational standpoint, the battery-driven discharge approach offers several advantages. It allows for the delivery of variable-energy pulses, providing flexibility to adjust the energy level based on the system's condition. Lower energy pulses can

be employed when the system is prone to short circuits, while higher energy pulses can be utilised to address specific mission requirements. This variability in thrust impulse bit opens possibilities for attitude manoeuvres and precise control of the spacecraft's trajectory [25]. Implementing battery-driven discharge for triggerless VATs provides a promising avenue for further research and development. It enables stable and variable-duration pulses, offering operational advantages and potential improvements over capacitor-based systems.

Acknowledgements

This work is supported by the UKSA through the Plasma thruster based Automated De-orbiting-Block system (PAD-B): UKSAG21_0071.

The authors would like to thank Dr Davina Di Cara, Directorate of Technology, Engineering & Quality- European Space Agency, for supporting earlier efforts related to this article.

The authors acknowledge the use of the IRIDIS High-Performance Computing Facility and associated support services at the University of Southampton, in the completion of this work.

Authors' contributions

J.S. wrote the main manuscript text, prepared the figures within the manuscript, designed, and manufactured the hardware for experimentation (electronics and VAT's), designed and conducted the experiments, processed experimental data. M.K. guided and supervised all work conducted by J.S. K.S. produced the data for Fig. 3. A.W. guided and supervised the work conducted by K.S. All authors reviewed the manuscript.

Funding

UKSA through the Plasma thruster based Automated De-orbiting-Block system (PAD-B): UKSAG21_0071.

Availability of data and materials

Available on request.

Declarations

Competing interests

The authors declare no competing interests.

Received: 21 August 2023 Accepted: 19 December 2023

Published online: 15 January 2024

References

1. CubeSat D (2022) Specification Rev. 14.1 The CubeSat Program, Cal Poly SLO CubeSat Design Specification Cal Poly-San Luis Obispo, CA Document Classification X Public Domain:
2. Morozov AI, Savelyev VV (2000). In: Kadomtsev BB, Shafranov VD (eds) Review of plasma physics, vol 21. Consultants Bureau, New York, p 203
3. Tummala AR, Dutta A (2017) An overview of cube-Satellite propulsion technologies and trends. *Aerospace* 4(4):1–30. <https://doi.org/10.3390/aerospace4040058>
4. Beilis II (2020) Plasma and spot phenomena in electrical arcs. *Springer Series on Atomic, Optical, and Plasma Physics*. Vol. 113, p 1003–1005
5. Beilis I (1996) Theoretical modeling of Cathode Spot Phenomena. *Handb Vacuum Arc Sci Technol* 208–256. <https://doi.org/10.1016/b978-081551375-9.50008-4>.
6. Keidar M, Schein J, Wilson K, Gerhan A, Au M, Tang B, Idzkowski L, Krishnan M, Beilis II (2005) Magnetically enhanced vacuum arc thruster. *Plasma Sources Sci Technol* 14(4):661–669. <https://doi.org/10.1088/0963-0252/14/4/004>
7. Polk JE, Sekerak MJ, Ziemer JK, Schein J, Qi N, Anders A (2008) A theoretical analysis of vacuum arc thruster and vacuum arc ion thruster performance. *IEEE Trans Plasma Sci* 36(5 PART 1):2167–2179. <https://doi.org/10.1109/TPS.2008.2004374>
8. Anders A, Brown IG, MacGill RA, Dickinson MR (1998) Triggerless triggering of vacuum arcs. *J Phys D* 31(5):584–587. <https://doi.org/10.1088/0022-3727/31/5/015>
9. Schein J, Qi N, Binder R, Krishnan M, Ziemer JK, Polk JE, Anders A (2002) Inductive energy storage driven vacuum arc thruster. *Rev Sci Instrum* 73(2 II):925. <https://doi.org/10.1063/1.1428784>
10. Pietzka M (2016) Development and Characterization of a Propulsion System for CubeSats Based on Vacuum Arc Thrusters. Ph.D. Thesis, Munich University, Munich, p 2–16. Available online: <http://dnb.info/1115728423>. Accessed 3 Nov 2020
11. Li YH, Pan JY (2019) Herdrich G (2020) Design and demonstration of micro-scale vacuum cathode arc thruster with inductive energy storage circuit. *Acta Astronaut* 172:33–46. <https://doi.org/10.1016/j.actaastro.2020.03.012>
12. Zolotukhin DB, Keidar M (2018) Optimization of discharge triggering in microcathode vacuum arc thruster for CubeSats. *Plasma Sources Sci Technol* 27:74001. <https://doi.org/10.1088/1361-6595/aacdb0>
13. Saddul K, Wittig A, Saletes J, Kim M (2022) End-of-life disposal of sub-3U CubeSat with a printed thin-film vacuum arc thruster. In: *International Astronautical Congress*. <https://eprints.soton.ac.uk/472810/>

14. IADC (2007) Inter-Agency Space Debris Coordination Committee, Space Debris Mitigation Guidelines. Issue 22. http://www.iadc-online.org/Documents/IADC-2002-01_IADC_Space_Debris_Guidelines_Revision_1.pdf
15. Nozette S (1995) The Clementine mission: past, present, and future. *Acta Astronaut.* [https://doi.org/10.1016/0094-5765\(94\)00181-K](https://doi.org/10.1016/0094-5765(94)00181-K)
16. Chen W, Jin Y, Zhao J, Liu N, Cui Y (2018) Nickel-hydrogen batteries for large-scale energy storage. *Proc Natl Acad Sci USA* 115(46):11694. <https://doi.org/10.1073/pnas.1809344115>
17. Spacewalkers Complete Multi-Year Station Battery Upgrades | NASA. (n.d.). Retrieved August 3 (2023) from <https://www.nasa.gov/feature/spacewalkers-complete-multi-year-effort-to-upgrade-space-station-batteries>
18. Knap V, Vestergaard LK, Stroe DI (2020) A review of Battery technology in cubesats and small satellite solutions. *Energies* 13(16):Art. No. 4097. <https://doi.org/10.3390/en13164097>
19. Zeng X, Li M, El-Hady A, Alshitari D, Al-Bogami W, Lu AS et al (2019) Commercialization of lithium battery technologies for electric vehicles. *Adv Energy Mater* 9(27):190061. <https://doi.org/10.1002/aenm.201900161>
20. Xiao C, Wang B, Zhao D, Wang C (2023) Comprehensive investigation on Lithium batteries for electric and hybrid-electric unmanned aerial vehicle applications. *Therm Sci Eng Progress* 38:101677. <https://doi.org/10.1016/j.tsep.2023.101677>
21. Balaram J, Aung MM, Golombek MP (2021) The Ingenuity Helicopter on the Perseverance Rover. In *Space Science Reviews* 217(4):56. <https://doi.org/10.1007/s11214-021-00815-w>
22. NovaCentrix. (n.d.). Metalon-JR-700LV-TDS, Retrieved (2023) August 3, from <https://www.novacentrix.com/datasheet/Metalon-JR-700LV-TDS.pdf>
23. Corning (2023) (n.d.). MACOR Machinable Glass Ceramic for Industrial Applications. Retrieved August 4, from <https://www.corning.com/media/worldwide/csm/documents/71759a443535431395eb34e91cb.pdf>
24. Geller RF, Yavorsky PJ (1945) Melting Point of Al₂O₃. *Alumina* 34(4):395–401
25. Gatsonis NA, Lu Y, Blandino J, Demetriou MA, Paschalidis N (2016) Micropulsed plasma thrusters for attitude control of a low-earth-orbiting cubesat. *J Spacecr Rockets* 53(1):57. <https://doi.org/10.2514/1.A33345>

Publisher's Note

Springer Nature remains neutral with regard to jurisdictional claims in published maps and institutional affiliations.